

# INTEGRATION OF RADARSAT-1 AND LANDSAT TM IMAGES FOR MINERAL EXPLORATION IN EAST OWEINAT DISTRICT, SOUTH WESTERN DESERT, EGYPT

T. M. Ramadan<sup>a</sup>, A. H. Nasr<sup>a</sup> and A. Mahmood<sup>b</sup>

<sup>a</sup>The National Authority for Remote Sensing and Space Sciences, Cairo, Egypt ramadan\_narss2002@yahoo.com

<sup>b</sup>Canadian Space Agency, Canada

**Keywords:** East Oweinat, Principal Component, Landsat TM, RADARSAT-1, Banded Iron Formation

## ABSTRACT

East Oweinat district is located in the south Western Desert of Egypt. It is mainly occupied by outcrops of Archean to Early Proterozoic rocks of high to medium metamorphic grade and younger granitoid rocks of calc alkaline and alkaline affinity. These rocks are unconformably overlain by Paleozoic and Mesozoic sediments as well as Quaternary deposits. Landsat TM images proved to be useful in surface mapping of lithologic and structural features in that area. RADARSAT-1 images reveal fluvial features beneath a surface cover of the desert sand. These features are not observable in Landsat TM images of similar resolution. In this work, the Principal Component Analysis (PCA) technique is used for merging RADARSAT-1 and Landsat TM images to enhance the interpretation of geological features. The data fusion produced a new data set of images showing enhanced subsurface structures such as foliation, faults and folds that control the distribution of the Banded Iron Formation and placer deposits in Quaternary paleo-drainages in the study district. The study demonstrates the utility of merging optical and radar remote sensing data for exploring mineral deposits in arid regions.

## 1. INTRODUCTION

East Oweinat district is located at the southwestern part of the Western Desert of Egypt between Lat. 22° 00' and 22° 15' N and Long. 25° 35' and 26° 05' E (Fig. 1). Previous studies (Klerx 1980, Richter and Schandelmier 1990, Said et al. 1998, Naim et al. 1998 and Khattab et al. 2002) studied the surface geology and mineral deposits of the study area. Khattab et al. (2002) suggested that the Banded Iron Formation (BIF) at El Oweinat area is represented by highly folded and faulted belt of Archean to Early Proterozoic age. Multi-sensor data combination is commonly used to generate a better imagery data set for visual interpretation or better feature space to extract more information for detection and classification (Klein 1993). El Baz and Robinson (1997), Robinson et al. (1999) and Ramadan et al. (2001). Pohl and Genderen (1998) used pixel based image fusion techniques for geological mapping and exploration of mineral and groundwater in arid regions. Le Moigene et al. (2001) have used a data fusion technique of SAR and Landsat images for enhancement of tropical land cover mapping. Several statistical/numerical methods have been proposed. They include arithmetic combination, Principal Component Analysis (PCA), high pass filtering, Intensity Hue Saturation, and wavelet transform.

This work focuses on the merging of RADARSAT-1 and Landsat TM data for geological mapping and mineral exploration in the study area. The PCA technique is used for merging these imagery data to enhance subsurface structures such as foliation and faults that control the distribution of BIF in the study area. The mineralogical studies for 15 samples from the investigated BIF were carried out.

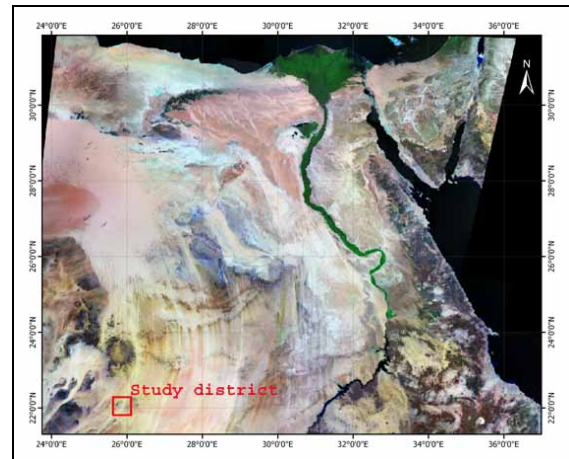


Figure. 1. Landsat TM image showing the location of the study district

## 2. METHODOLOGY

Two sets of remote sensing data were used. The first is the Landsat TM image and the second is the Radarsat-1 data. A Landsat TM image (Path: 178, Row: 45) acquired on October 1984. The image has been geometrically and radiometrically corrected (Fig. 2). Three bands (7, 4, 2) have been selected since they contain most of the information about the surface geological features of the study area.

The spatial resolution is 30 x 30 m and the image size is 1841 x 1869 pixels. The image was processed using the ERDAS Imagine, version 8.3 software, on a Sun spark workstation. The second set is a RADARSAT-1 scene was acquired on Sep. 16, 1998. Radarsat is a polar orbiting satellite that carries an imaging radar sensors (Parashar et al. 1993). The image was acquired from the Standard Beam 5, which features a swath width of 100 km, spatial resolution 25 m, and incidence angle of 39° at the scene centre.

Our proposed scheme aims at merging the Landsat TM and Radarsat images using the PCA transform in order to produce a 25 m merged image (Fig. 3). The PCA is a method of reducing the data dimensions into a fewer linear combinations of spectral bands. The output linear combinations are new dimensions, which are non-correlated and often more interpretable than the original spectral data (Jensen 1996). With this transform, the multispectral image (TM data) is transformed into the PCA single components. The principle is based on the computation of the covariance matrix and its diagonalization by finding corresponding eigenvalues and eigenvectors. The first eigenvector (or principal component) is a linear combination of the initial bands and usually contains more than 90 % of the information contained in all channels. This value is replaced by the matched RADARSAT-1 image and the inverse transform is applied to get the fused image after being rescaled, as shown in a schematic diagram in Figure (4). This fusion steps can be summarized as follows: i) Radarsat and Landsat TM images are co-registered using different tie points. Then they were resampled to 25 m using the nearest neighbor technique. ii) Transform the TM image into the PCA components. iii) Perform histogram match between the Radarsat image and the first principal component of the TM image. iv) Replace the first PC with the matched Radarsat image. v) Perform the inverse transforms, and rescale the output image to the dynamic range (0-255). vi) Generate the final output fused image.

### 3. GEOLOGICAL SETTING

The investigated area is occupied largely by Archean to Early Proterozoic rocks of high to medium metamorphic grade and younger granitoid rocks of calc alkaline and alkaline affinity. These rocks are unconformably overlain by Paleozoic and Mesozoic sediments as well as Quaternary deposits. The Archean to Early Proterozoic metamorphic rocks are represented by: mafic-ultramafic associations, gneisses group (felsic granulite, quartz feldspathic gneisses, quartzite calc-silicate rocks) and BIF. The gneissic and migmatite rocks are composed of alternating melano and leucocratic bands. They are represented by para and orthogneisses and showing intense deformation manifested by folding and faulting with at least four deformation phases (Said, et al., 1998). Anatectic features are well-defined by typical migmatization mega-structures, e.g. lit by lit and rare pygmatic structures with growth of orthoclase crystals in the gneissic rocks.

Several BIF are hosted in the gneissic rocks and outcropping as small low hills (Fig. 5a). Quaternary deposits cover vast areas as sand sheets and sand dunes (Fig. 5b).

It is worth mentioning that the aeolian sand dunes in the study area appear as linear and anchored dunes and displaying unimodal distributions.

The sands of anchored dunes are generally moderately sorted, but still better than those of the interdunal area. The medium-grained sands are mostly subrounded, while the fine sands are subangular.

The study area is characterized by the presence of BIF associated with the gneissic rocks, which form ridges and isolated hills and have northly to northly west dips at angles of 30° to 70°. Locally, some beds strike NNE-SSW and NW-SE, and dip WNW and NE at angles of 40° to 60°. The BIF with the latter trends is generally thinner in thickness than those of other trends. This formation varies in thickness from a few meters to 100 m. and extends to 7.0 km as discontinuous along-strike beds. The repetition of BIF bands is due to isoclinal folds which plunge to the west. The ore minerals are represented by hematite and goethite as major constituents associated with magnetite and rare sulphides (Naim et al. 1998). The chemical analyses for major oxides reveal that SiO<sub>2</sub> and Fe<sub>2</sub>O<sub>3</sub> are the two most abundant oxides (Khatab et al. 2002). They vary from 37.02 % to 60.3 % and from 32.5 % to 61.06 % respectively.

## 4. RESULTS AND DISCUSSION

False colour Landsat TM image (Bands 7,4,2 in R, G, B) of the study area was used for surface lithological and structural analysis. The processed Landsat TM ratio image (5/7, 5/1 and band 4 in R,G, B respectively) demonstrated that the metamorphic rocks appear in red colour, the Paleozoic and Mesozoic sediments appear in green and the Quaternary sediments rocks appear in blue. The metamorphic rocks are represented by: i) mafic-ultramafic granulite and ii) orthogneisses (felsic granulite), paragneisses (quartzite, quartz-feldspar gneiss) and BIF. These rocks are intruded by younger granitic rocks with sharp intrusive contact. These rocks are unconformably overlain by the Gifl Formation (Paleozoic), Abu Ras Formation ( Mesozoic) and Quaternary sediments (Fig. 6).

The most important finding of this study is the appearance of features beneath the sand surface on the merged Landsat TM and Radarsat images (referred to in the rest of this paper as the merged image). These features are not observable at all on the Landsat TM images of similar spatial resolution (Figs. 2 and 3), signifying the effectiveness of multisatellite image analysis in geological survey. Based on the interpretation of the merged images, new geological and structural maps were attempted that are summarized below with regards to the drainage pattern, lithological and structural features.

### 4.1. The drainage pattern

The merged image has brought up the buried drainage pattern at the study area in a most revealing manner. This feature has no surface expression and is not visible on the Landsat TM image (Figs. 2 and 3). Excavations in this area indicated that the fine-grained sand dunes in this locality have a thickness of only 0.5 m - 1 m (Fig. 5a) and given the aridity of the soils permitted radar subsurface penetration and capturing of the feature in the signal. Two major NE and SE trending drainage lines are revealed by RADARSAT-1 data to lead into the northern and southern sides of the study area. The northernmost drainage system appears to trend NNE and measure about 30 km in length (W1, Figs 2 and 3).

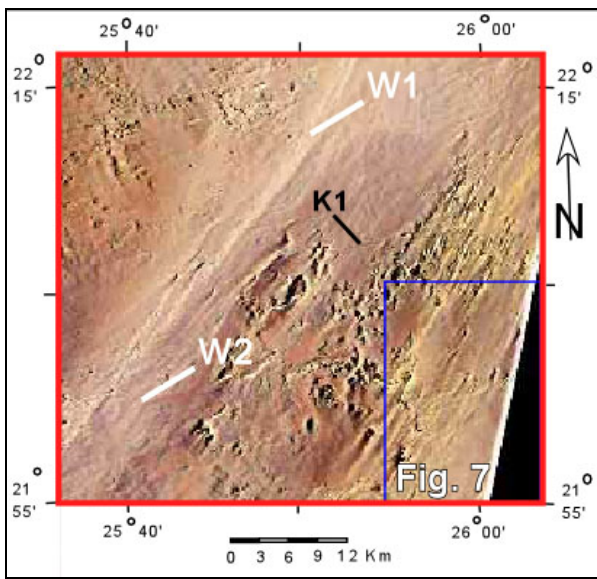


Figure. 2. Landsat TM image (Bands 7,4,2) for the study district

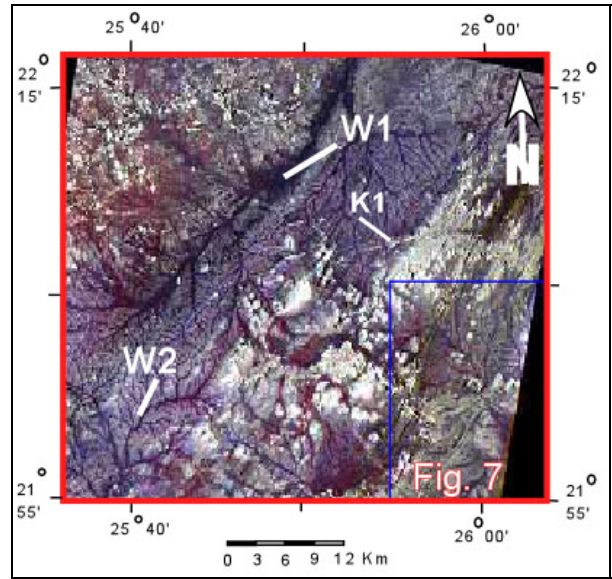


Figure. 3. Landsat / RADARSAT-1 image for the study district

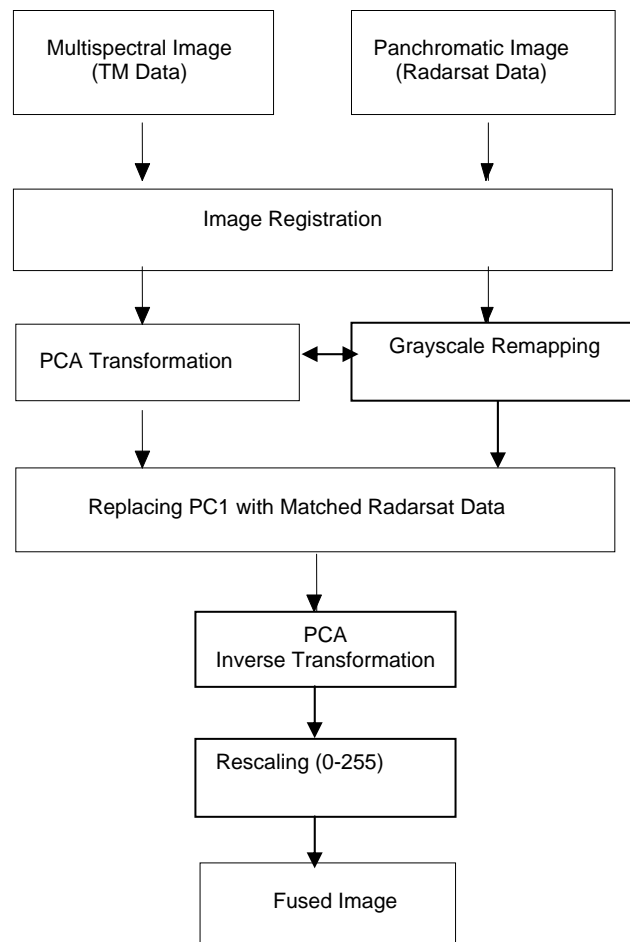


Figure. 4 . Schematic diagram of the fusion technique

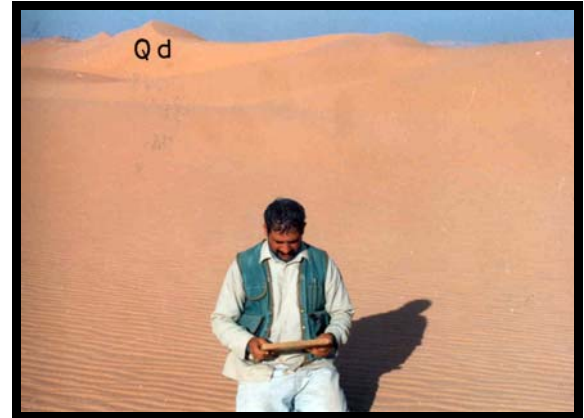
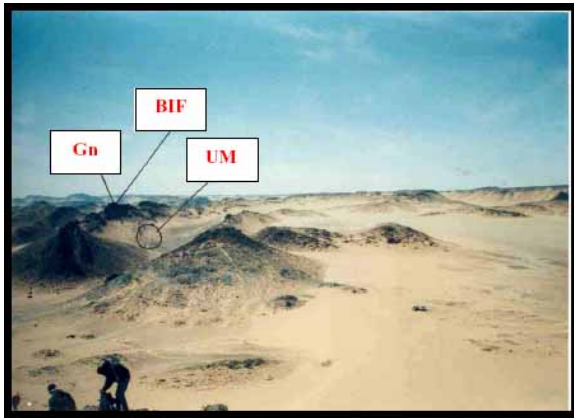


Figure. 5a. Sand sheets partly covered the BIF, the gneissic rocks (Gn) and the ultramafic rocks (UM) in the central part of the study district.

Figure. 5b. Sand dunes (Qd) cover the central part of the study district.

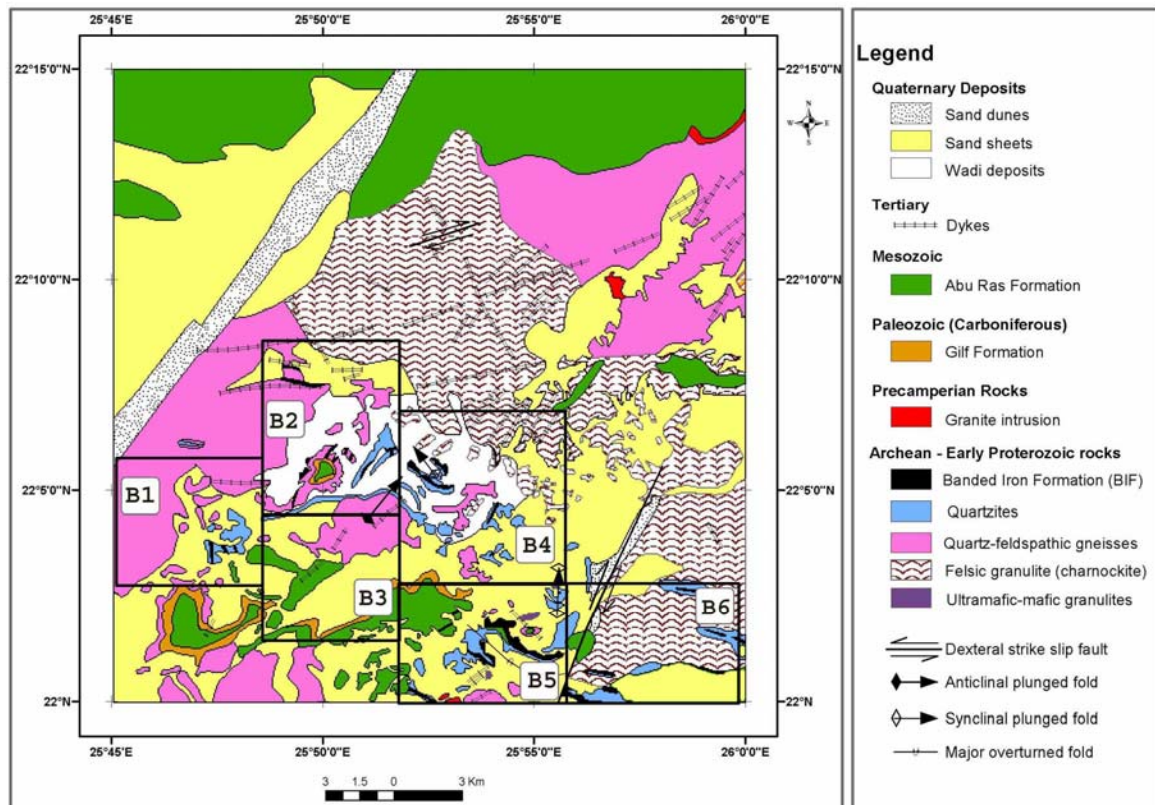


Figure. 6. Geological map for the study district (Modified after Khattab et al. 2002).

The southernmost valley in this region is composed also of a Very broad channel and is aligned in S-SE direction (W2, Figs. 2, and 3).

#### 4.2. Lithologic features

Figure 7-a is the Landsat subscene of the southeastern part of the study area. It shows the bedrock covered by sand sheet and sand dunes (indicated by arrows). The highly weathered bedrock outcrops as small low lying hills in the desert landscape. The merged image (Fig. 7-b) reveals the bedrock features in much more detail. On the south eastern part of the image there is an oval-shaped stock of probably granitoid rocks with total approximate area of  $7 \times 5 \text{ km}^2$ . This stock is fragmented and the fragments are denoted as S1, S2, S3, S4, and S5 in Fig. 7-c.

There are three major E-W faults as well as two NW-SE faults traversing the granitoid stock (Fig. 7-b). These are marked as red lines in Fig. 7-c. The stock and the faults are completely invisible in the Landsat image (Fig. 7-a) as they are also covered with sand sheets transported across the granitoid stock from north to south. The dominant radar signature of the fragmented granitoid stock is bright where the linear features (faults) appear in dark. The dominant material in the faults are mainly clays (fine-particle material) derived from the weathering of the granitic rocks in the Tertiary period. This fine-particle material returns dark signature in radar images mainly due to their smooth surfaces. This is in agreement with results given by Schaber et al., (1996). This dark signature contrasts with the common bright radar signature of the granitoid stock because of the surface roughness of the latter. The fine particles material (saprolites) was formed during tropical wind weathering and semi-tropical interludes (mostly Tertiary).

The particles tend to concentrate within the granite stocks and to be preserved, along with the blown sand, in various topographic traps (i.e., fractures) beneath the weathering cap and possibly extending down from the cap. Chemical weathering, on the other hand, turns the feldspars into clays, leaves the quartz behind, and preserves the original rock texture. The bedrock in the central part of the study area are cut by several basic and acidic dykes, also covered by recent sands (K1 in Fig. 2). The basic dykes are mainly doleritic in composition, with ENE-WSW trend. The acidic dykes are younger than the basic dykes and are mainly felsitic and trachytic in composition. They extend for several km. in a NE-SW trend and are partly covered with recent sands. The merged image (Fig. 3) distinctly shows some of these dykes beneath the recent sands.

#### 4.3. Structural features

Based on field studies carried out by Said et al. (1998) and Khattab et al., (2002) as well as the interpretation of the merged image. Three deformation events were recognized in the study area: 1): Emplacement of S-verging ophiolite napes: 2) E- W shortening which produced N-S trending folds followed by NNW-SSE thrust faults and development of E-W trending sinistral strike slip faults (Fig. 6). The merged image revealed some subsurface Precambrian structures such as foliations, folds and faults that control the distribution of the gneissic rocks and associated BIF in the study area.

These are mostly covered with recent sands (Figs. 7a, 7b and 7c). The structural features are defined by trends of alternating dark and bright bands which correspond to transposed bedding and metamorphic layering in the investigated gneissic rocks (M, Figs. 7b and 7c). Also, numerous folds are recognized on the merged image (Figs. 7b and 7c). These folds are dominantly tight, plunge to the south and have sub-vertical axial surfaces.

The core of the unmapable folds are frequently intruded by granitic masses (Figs. 7b and 7c). Fold closures are defined by curvatures in these bands at the eastern side of the mapped area (Figs. 7b and 7c). The planar view geometry of fold hinge zones (angular, rounded or box) is well-defined on the merged image. However, determining the three-dimensional geometry of folds (plunge of hinge line, attitude of the axial surface, and attitude of the limbs) is not possible based on the image alone. Moreover, this merged image enhances the relatively younger structures such as normal and strike slip faults in the Paleozoic and Mesozoic sediments, beneath a dry sand cover at the northern part of the study area (Figs. 7b and 7c). These features have no surface expression and are not visible in the Landsat TM image alone (Fig. 7a).

#### 4.4. Mineral deposits

The study area is characterized by the presence of widely distributed BIF with huge tonnages, as well as economic heavy minerals in the placer deposits. The BIF are hosted in the gneissic rocks and forms ridges and isolated hills (Fig. 5a). In the present work, the mineralogical studies for representative samples from the investigated BIF indicate that they consist of intercalation of iron oxides, quartz, pyroxenes, amphiboles associated with minor siliceous material. Iron oxides are represented by magnetite, hematite and goethite.

The presence of hypersthene and diopside reflect the high grade metamorphism of this rock, where the presence of tremolite-actinolite points to retrograde metamorphism. As in the case with other bedrock units described above, BIF is also mostly covered with recent sands (Fig. 5b) and located in the south eastern part of the study area. The merged image enhances the subsurface structures such as foliation, folds and faults that control the distribution of the BIF in the study area. These structures with southeasterly and southwesterly extensions are defined by trends of alternating dark and bright bands which correspond to transposed bedding and metamorphic layering in the investigated gneissic rocks. They consist of strongly folded and faulted beds striking E-W and NE-SW. Excavations in this area indicated that the BIF is present underneath the dry sand sheets at depths of 0.6 m to 1 m. Therefore, the southern and southeastern parts are located in the areas: B1, B2, B3, B4, B5 and B6, (Fig. 6) and can be considered as promising territories for further exploration and target Fe-rich areas.

## CONCLUSIONS

An approach for integrating Landsat TM and Radarsat images was developed to assist geological mapping and mineral exploration. RADARSAT-1 image of the Gabal Kamel-East Oweinat area reveals fluvial features beneath a surface cover of desert sand. These features are not observable in Landsat TM images at similar resolution.

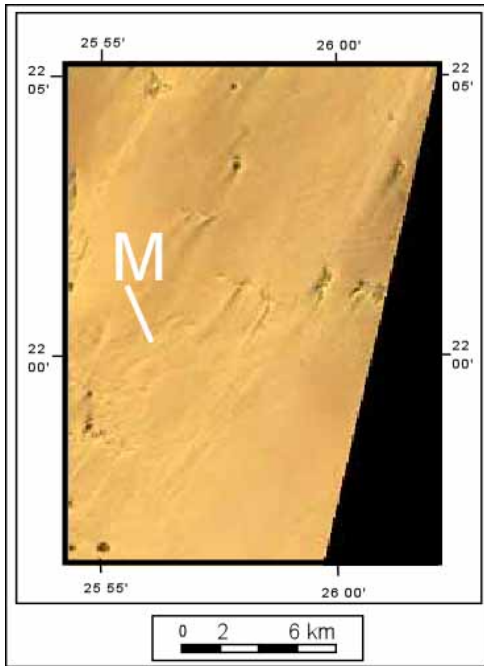


Figure. 7a. Landsat TM image (Bands 7,4,2) for the southeastern part of the study area

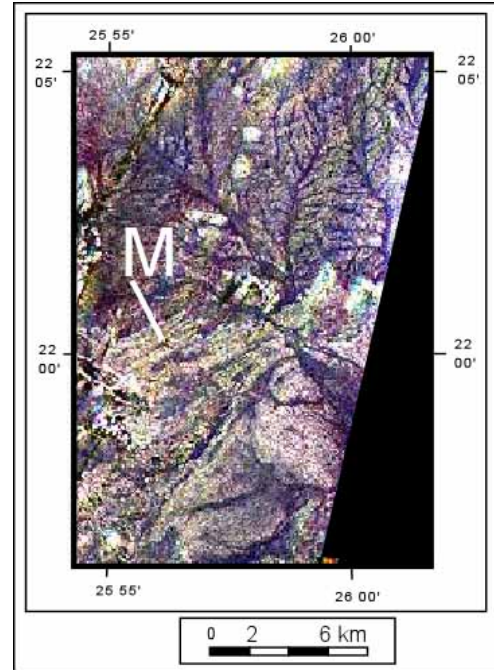


Figure. 7b. Landsat TM / RADARSAT-1 image for the southeastern part of the study district

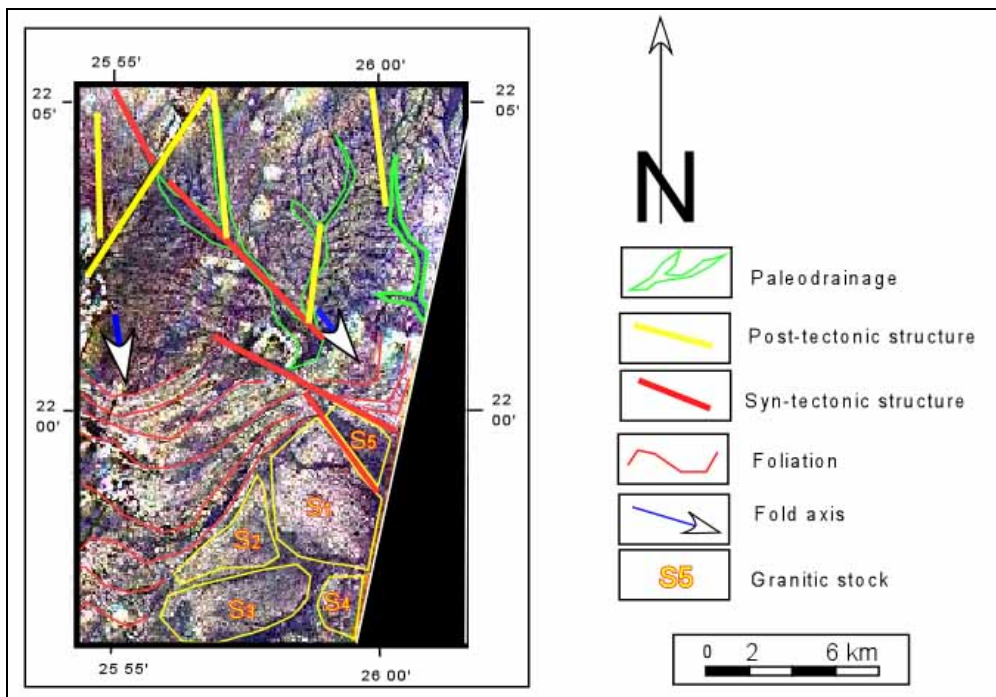


Figure. 7c. Photo-geological map interpreted from Landsat TM / Radarsat image, showing the subsurface features at the southeastern part of the study district

Principal component analysis technique is used for merging the two data sets. The product improves visual detection of subsurface structures such as foliations, folding and faults that control the distribution of the BIF in the study area. Those features are covered with sand sheets, dunes and wadi alluvium, which makes them almost undetectable in Landsat TM data. Moreover, the merging of the two data sets reveals drainage pattern and recent structures. These features are valuable for exploration of mineral deposits such as Banded Iron Formation (BIF) and heavy minerals in placer deposits in the investigated district and similar regions. The southern and southeastern parts of the study area include the areas: (B1 – B2), (B3-B4) and (B5-B6) and can be considered as promising territory for further exploration. Also, the merged image enhanced subsurface structures such as faults that control the distribution of placer deposits in paleo-drainages in the studied district.

This study demonstrates the importance of using proposed remote sensing technique (merging landsat TM and Radarsat data) in mineral exploration to detect the covered mineral deposits in the East El Oweinat district.

#### ACKNOWLEDGEMENTS

The authors would like to thank Prof. Mohammed Shokr, Environment, Canada and Prof. Atef Cherif, Chairman of The National Authority for Remote Sensing and Space Sciences, Egypt, for their sincere help and invaluable comments and suggestions. Thanks also to Mr. Atef Omar, EGSM for fruitful discussion.

#### REFERENCES

- El Baz F. and Robinson C. A. 1997. Inferences of Paleotopography from Palaeochannels Revealed by SIR-C Data in the Western Desert of Egypt: Implications to Sand Dune Accumulation. Proc. ERIM 12<sup>th</sup> ERIM Symposium on Geologic Remote Sensing. Colorado, Vol. 1, pp. 469-476.
- Hamdan, M. A., 2003. Textural, mineralogical and geochemical characteristics of the Aeolian dune sand of Gilf Kiber-Gebel Uwinat area, southwestern Egypt. Fifth International Conference on the geology of the Middle East, Cairo, Egypt. pp. 379-392.
- Jensen, J. R., 1996. *Introductory Digital Image Processing: A Remote Sensing Perspective*. Second ed. Upper Saddle River, NJ: Prentice Hall.
- Khattab, M. M., Greiling, O. R., Khalid, A. M., Said, M. M., Kontny, A., Abu Salem, A. O., El Kady, M. F., Attia, M. N. and Shaaban, G. M., 2002. Al Uwaynat Banded Iron Formation ( SW Egypt) distribution and related gold mineralization. *Annals Geol. Surv. Egypt*, V. 25, pp.343-364.
- Klerkx, J., 1980. Age and metamorphic evolution of the basement complex around Gabal Al Uwaynat. In Salem, M. J. and Busserawil M.T. (eds). *The Geology of Libya Academic press*. V.3. pp.901-906.
- Klein, L. A., 1993. *Sensor and Data Fusion Concepts and Applications Washington. SPIE Optical Engineering Press*, pp 31.
- Le Moigne, J., Laporte, N. and Netanyahu, N. S., 2001. Enhancement of Tropical Land Cover Mapping with Wavelet-Based Fusion and Unsupervised Clustering of SAR and Landsat Image Data. Proc. of SPIE, The 8<sup>th</sup> International Symposium on Remote Sensing, Toulouse, France. pp. 190-198.
- Naim, G. M., Khalid, A. M., Said, M. M., Shaaban, G. M., Hussein, A. M. and El Kady, M. F., 1998. Banded Iron Formation Discovery at west of Gabal Kamel and its gold potential. Western Desert. Egypt. *Annal. Geol. Surv. Egypt*. Vol. 21, pp.303-330.
- Parashar, S., E. Langham, J. McNally, and S. Ahmed, 1993. RADARSAT-1 mission requirements and concepts. *Canadian Journal of Remote Sensing*,. Vol. 19. pp. 280-288.
- Pohl, C. and Van Genderen, J. L., 1998. Multisensor Image Fusion in Remote Sensing: Concepts, Methods and Applications. *International Journal of Remote Sensing*, Vol. 19, No. 5, pp. 823-854.
- Ramadan, T. M., Abdelsalam, M. G. and Stern, R. S., 2001. Mapping gold bearing massive sulfide deposits. in the Neoproterozoic Allaqi Suture, SE Egypt- with Landsat TM and SIR-C/X SAR imagery. *Journal of Photogrammetric Engineering and Remote Sensing (PE&RS)*, Vol. 64, No. 4, pp. 491-498
- Richter, A. and Schandelmieir, H., 1990. Precambrian basement Inliers of Western Desert, Geology, Petrology and Structural Evolution. In Said, R.(ed). *The Geology of Egypt*, A.A. Balkema, 1990, pp. 185-200.
- Robinson, C. A., El Baz, F. and Singhroy, V. H., 1999. Subsurface Imaging by Radarsat: Comparison with Landsat TM Data and Implications for Groundwater in Selima Area, Northwestern Sudan. *Canadian Journal of Remote Sensing*, Vol. 25, No. 3, pp. 268 – 277.
- Schaber G. G., McCauley, J. F., Breed, C. S. and Issawi, B., 1996. The application of Space Shuttle Radar-C Data (SIR – C/X –SAR) to geologic studies of Bir Safsaf, Egypt. Proc. Geol. Surv. Egypt Cenn. Conf. (1996), pp.727-758.
- Said, M. M., Khalid, A. M., El Kady, M. F., Abu Salem, A. O. and Ibrahim, S. M. (1998). On the structural evolution of the Banded Iron Formation of Gabal Kamel and its role in the gold mineralization. *Annal, Geol. Surv Egypt*. V. 21. pp.345-352.